Mechanism and Machine Theory 44 (2009) 1156–1175

Contents lists available at ScienceDirect

Mechanism and Machine Theory

journal homepage: www.elsevier.com/locate/mechmt

Kinetostatic modeling of 3-RRR compliant micro-motion stages with flexure hinges

Yuen Kuan Yong [a,*], Tien-Fu Lu [b]

[a] School of Electrical Engineering and Computer Science, The University of Newcastle, Callaghan, NSW 2308, Australia
[b] School of Mechanical Engineering, The University of Adelaide, SA 5005, Australia

ARTICLE INFO

Article history:
Received 9 February 2007
Received in revised form 10 June 2008
Accepted 8 September 2008
Available online 5 November 2008

Keywords:
Kinetostatic model
3-RRR
Compliant mechanism
Flexure hinge
Finite-element-analysis

ABSTRACT

This paper presents the derivation of the kinetostatic model of a flexure-based 3-RRR compliant micro-motion stage. The kinetostatic model has closed-form equations and flexure hinge compliances are one of the variables in the model. Researchers have an option of selecting the most suitable flexure hinge compliance equations to calculate the kinetostatics of the stage. Two cases are studied where two kinetostatic results are obtained using two different sets of flexure hinge equations. The kinetostatic results are compared to the finite-element-analysis results to verify their accuracies.

1. Introduction

Micro-motion stages have emerged as an important technological advancement in the past three decades. The significance of this advancement is highlighted in many applications where the positioning of components with micrometer or nanometer accuracy is required. Examples include the positioning of samples in a scanning-electron-microscope (SEM), the alignment of fibre-optics and lasers, the positioning of masks in lithography, the manipulation of cells in micro-biology and the manipulation of micro-scale components in micro-assembly. Most of the micro-motion stages are designed based on the compliant mechanism concept. Compliant mechanisms generate their motions through elastic deformations. Compliant mechanisms eliminate problems such as wear, backlash, friction and needs for lubrication. Piezoelectric stack actuators, hereafter referred to as piezo-actuators, are commonly used to provide fine resolution of input displacements to compliant mechanisms.

Kinematic, static and dynamic models are needed to analyze and to synthesize the behavior of a particular compliant stage design. The pseudo-rigid-body-model (PRBM) method is commonly used to predict the displacements of compliant mechanisms with circular flexure hinges. The PRBM models a flexure hinge as a revolute joint (one-DOF) with an attached torsional spring. Although the PRBM method is effective and it simplifies the model of compliant mechanisms, the PRBM suffers some inaccuracies when it ignores the Δx- and Δy-deformation of flexure hinges [1–3] (see Fig. 1).

The kinetostatic model allows the fulfillment of both the kinematics and the force design criteria of micro-motion stages. A precise kinetostatic model of compliant micro-motion stages will benefit researchers in at least the design phase where a good estimation of kinematics, workspace or stiffness of a micro-motion stage could be realized. Jouaneh and Yang [4] derived a kinetostatic model to predict the displacement and stiffness of a one-DOF, vertical motion compliant stage.

* Corresponding author. Tel.: +61 249216438; fax: +61 249601712.
E-mail address: yuenkuan.yong@newcastle.edu.au (Y.K. Yong).

0094-114X/$ - see front matter Crown Copyright © 2008 Published by Elsevier Ltd. All rights reserved.
doi:10.1016/j.mechmachtheory.2008.09.005

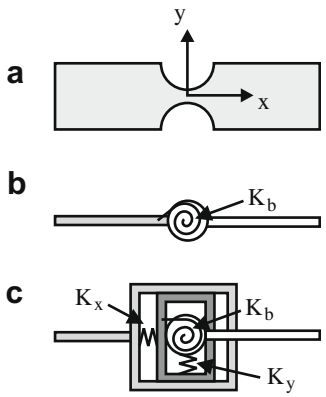

Fig. 1. (a) Flexure hinge. (b) One-DOF model (PRBM). (c) Three-DOF model [19].

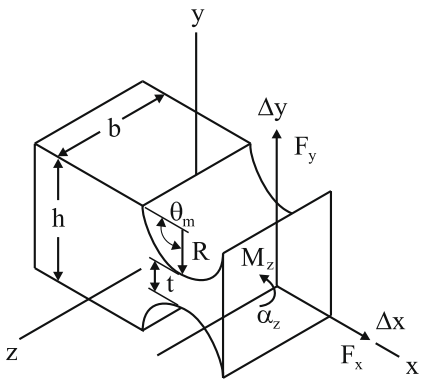

Fig. 2. Schematic of flexure hinge with dimensions, local coordinate, applied forces/moments and displacements.

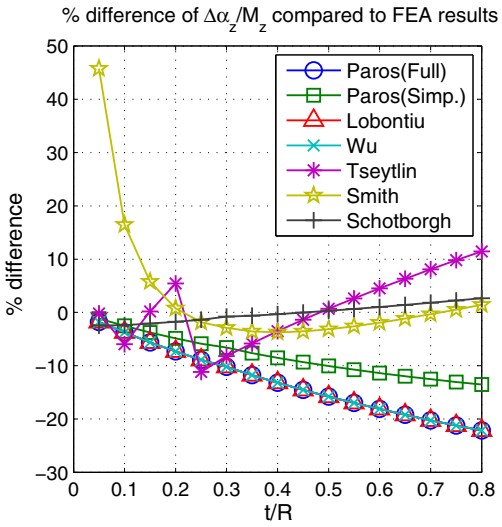

Fig. 3. Differences of various flexure hinge equations, $\Delta\alpha_z/M_z$ when compared to FEA results. These flexure hinge equations can be obtained in [15,18,23,24,11,14].

The developed equations modeled flexure hinges as having multi-DOF, which are the Δx-, Δy- and $\Delta\alpha_z$-deformation. The analytical results were in close agreement with the FEA results. However Jouaneh and Yang's paper focused only on the modeling of a one-DOF compliant mechanism. It was unclear if their modeling method would be applicable on compliant mechanisms, which have more than one-DOF such as 3-RRR compliant micro-motion stages. Lobontiu and Garcia [5] formulated an analytical method for displacement and stiffness calculations of a one-DOF planar compliant mechanisms with flexure hinges. The closed-form formulations were based on Castigliano's second theorem which considered all three in-plane compliances of hinges. The closed-form equations were expressed as a load–deformation/displacement relationship. Park and Yang [6] derived a kinetostatic model using the Castigliano's second theorem for a six-DOF compliant mechanism. The flexure hinges were modeled to have multi-DOF. The relationship between the input and the output displacements

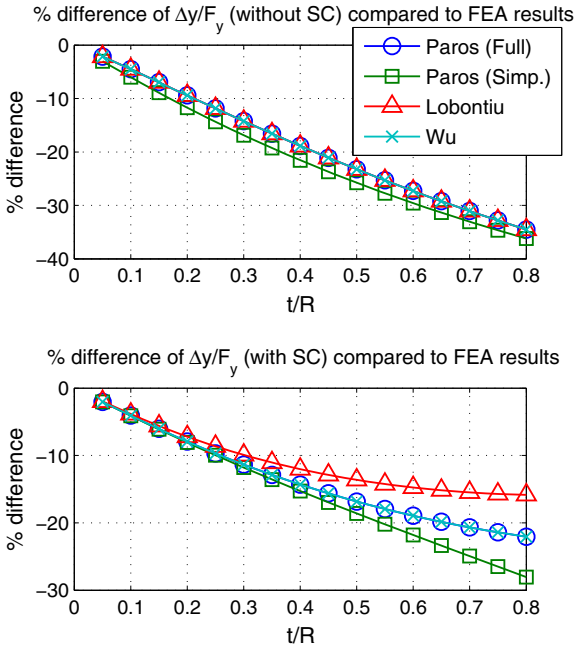

Fig. 4. Differences of various compliance equations, $\Delta y/F_y$ when compared to FEA results. SC is referred to shear compliance. These flexure hinge equations can be obtained in [15,18,23].

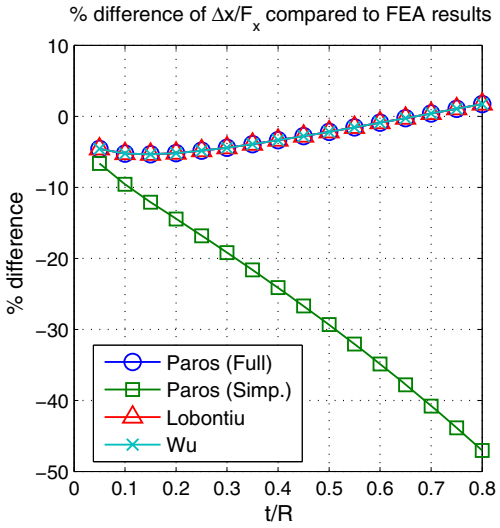

Fig. 5. Differences of various compliance equations, $\Delta x/F_x$ when compared to FEA results. These flexure hinge equations can be obtained in [15,18,23].

was also derived. They compared the predicted displacements with that of the FEA results and the differences are within 29%. Stiffnesses of the compliant mechanism were not verified with FEA models. Choi et al. [7] derived a formulation using the Lagrange's equation to predict the amplification ratio of a one-DOF compliant mechanism with circular flexure hinges. They modeled flexure hinges to have multi-DOF. It was unclear if their modeling method would be applicable on 3-RRR compliant micro-motion stages.

Few researchers derived kinetostatic models for 3-RRR micro-motion stages. Ryu et al. [8] developed a $XY\theta$ compliant stage which was driven by three piezo-actuators. The topology of this stage is similar to a 3-RRR compliant structure except it consists of a double compound lever at each of the input links. They formulated a kinetostatic model to describe the relationship between input and output displacements, and stiffnesses of the stage by modeling flexure hinges to have multi-DOF. They presented methodology of deriving the kinetostatic model is complicated and involves an intensive number of coordinate transformations. Pham and Chen [9] derived analytical models to estimate the output stiffnesses of a three-DOF translational flexure parallel mechanism (FPM). This FPM consists of three double compound linear structures (one-DOF mechanism) and three 3-RRR compliant mechanisms (three-DOF mechanism) in order to achieve three translational DOFs. The method of deriving the stiffness model involves an intensive number of transformation matrices. This method could lead to complications and difficulties when applied to other mechanisms. The input stiffness of the FPM was not presented and it is not clear if this methodology can be used to estimate the input stiffness of compliant mechanisms. The prediction of the input stiffness is particularly important for piezo-driven compliant mechanisms because the maximum displacement of a piezo-actuator is governed by the structural input stiffness. High input stiffness will reduce the maximum displacement of a piezo-actuator, which leads to the reduction of workspace of compliant mechanisms.

As a conclusion, the previously derived kinetostatic models for 3-RRR micro-motion stages are either complicated or do not demonstrate the capability of estimating the input stiffness of the compliant mechanisms.

This paper presents a simple, closed-form kinetostatic model of 3-RRR compliant micro-motion stages which can be used to predict the kinematics, and both the input and output compliances/stiffnesses of compliant mechanisms. Flexure hinges are modeled as having three-DOF due to the fact that the 3-RRR compliant stage is a planar stage. Out-of-plane compliances are very small for thick hinges (b is large) and are neglected. The closed-form kinetostatic model is expressed in terms of flexure hinge compliances, material properties and geometrical parameters. Various flexure hinge compliance equations were derived to predict the deformation and stiffness of a circular flexure hinge [10–15]. Most of the previously derived kinetostatic models were obtained using flexure hinge compliance equations derived by a particular research group such as Paros and Weisbord [15]. However, depending on the geometrical ratio of flexure hinges, t/R (see Fig. 2 for hinge geometries), some of these methods are more accurate than others [16,17]. Comparisons of results of various flexure hinge equations were carried out by the authors to support the above statement. FEA (ANSYS) results were used as a benchmark for the comparison. The differences between the results of flexure hinge equations and the FEA are shown in Figs. 3–5. These figures show that flexure hinge compliances determined using any single particular method may not be suitable for a large range

Table 1
Link length, flexure hinge dimensions and material properties of the 3-RRR compliant micro-motion stage

Material properties										
E										71.7 GPa
Poisson's ratio, v										0.33
Link length (mm)		l_1			l_2		l_3	l_4	l_5	l_6
		47.9			22.2		0	30	4	12
Flexure hinge (mm)	t_1	t_2	t_3	R_1	R_2	R_3	t_1/R_1	t_2/R_2	t_3/R_3	b
	0.84	0.7	0.5	1.1	1.87	3	0.764	0.374	0.167	12.7

Table 2
Flexure hinge equations chosen for Case 1 and Case 2 for the kinetostatic derivation of the 3-RRR micro-motion stage

	t/R	$\Delta\alpha_z/M_z$	$\Delta y/F_y$ (without shear compliance)	$\Delta x/F_x$
Case 1				
Flexure hinge 1	0.764	PW (full)	PW (simplified)	PW (simplified)
Flexure hinge 2	0.374	PW (full)	PW (simplified)	PW (simplified)
Flexure hinge 3	0.167	PW (full)	PW (simplified)	PW (simplified)
Case 2				
Flexure hinge 1	0.764	Schotborgh et al. [14]	Lobontiu [18]	PW (full)
Flexure hinge 2	0.374	Schotborgh et al. [14]	Lobontiu [18]	PW (full)
Flexure hinge 3	0.167	Schotborgh et al. [14]	Lobontiu [18]	PW (full)

PW is referred to Paros and Weisbord [15].

of t/R ratio. Since flexure hinge compliances are one of the variables in the kinetostatic model derived in this paper, the most suitable flexure hinge compliance equations can be chosen based on the t/R ratio of hinges to calculate the kinetostatic of 3-RRR mechanism accurately. Two cases are studied where two kinetostatic results are obtained using two different sets of flexure hinge compliance equations that derived previously by various research groups. The kinetostatic results of Case 1 were calculated by deliberately choosing the flexure hinge equations which have large differences when compared to the FEA results (refer to Figs. 3–5). Meanwhile, the kinetostatic results of Case 2 were obtained by choosing the flexure hinge equations which have small differences (refer to Figs. 3–5). Results of the kinetostatic models are compared to that of the FEA in order to verify their accuracies, and the differences are discussed.

2. Derivation of the kinetostatic model

The kinetostatic model of a 3-RRR micro-motion stage is shown below (refer to nomenclature in Appendix A for the definition of symbols),

Table 3
Design guideline of choosing a flexure hinge equation for a particular t/R range [16]

Research	α_z/M_z	% Error			$\Delta y/F_y$ (with SC)	% Error			$\Delta x/F_x$	% Error		
Group	t/R range	Min.	Max.	Ave.	t/R range	Min.	Max.	Ave.	t/R range	Min.	Max.	Ave.
PW[a] (full)	$0.05 \leqslant t/R < 0.1$	1.8	5.0	3.5	$0.05 \leqslant t/R \leqslant 0.1$	2	4	3.1	$0.25 \leqslant t/R \leqslant 0.65$	0.3	4.9	2.4
PW[a] (simpl.)	$0.05 \leqslant t/R \leqslant 0.2$	1.2	4.9	3.1	$0.05 \leqslant t/R \leqslant 0.1$	3	5.6	4.3	Not recommended			
Lobontiu	$0.05 \leqslant t/R < 0.1$	1.8	5.0	3.5	$0.05 \leqslant t/R \leqslant 0.1$	2	3.9	2.9	$0.25 \leqslant t/R \leqslant 0.65$	0.3	4.9	2.4
Wu and Zhou	$0.05 \leqslant t/R < 0.1$	1.8	5.0	3.5	$0.05 \leqslant t/R \leqslant 0.1$	2	4	3.1	$0.25 \leqslant t/R \leqslant 0.65$	0.3	4.9	2.4
Tseytlin	$0.4 \leqslant t/R \leqslant 0.6$	0.7	4.5	2.5	NA	NA	NA	NA	NA	NA	NA	NA
Smith	$0.2 \leqslant t/R \leqslant 0.65$	0.8	3.7	2.4	NA	NA	NA	NA	NA	NA	NA	NA
Schotborgh	$0.05 \leqslant t/R \leqslant 0.65$	0.03	2.5	1.2	NA	NA	NA	NA	NA	NA	NA	NA
This article	NA	NA	NA	NA	$0.05 \leqslant t/R \leqslant 0.8$	0	2.7	0.07	$0.05 \leqslant t/R \leqslant 0.8$	0	1.1	0.08

[a] Paros and Weisbord.

Table 4
Case studies – analytical matrices of the kinetostatic model of the 3-RRR micro-motion stage

	Analytical results		
Case 1			
$\mathbf{C}_{o,F_o}$	10.486	0	0
(μm/N, μrad/N	0	10.486	0
μm/Nm, μrad/Nm)	0	0	24,747
$\mathbf{C}_{o,F_{in}}$	0.810	0.229	−1.039
(μm/N, μrad/N)	0.732	−1.068	0.335
	−30.924	−30.924	−30.924
$\mathbf{C}_{in,F_{in}}$	0.152	−0.018	−0.018
(μm/N)	−0.018	0.152	−0.018
	−0.018	−0.018	0.152
$\mathbf{J}_{analytical}$	4.749	1.345	−6.093
	4.294	−6.260	1.965
	−266.749	−266.749	−266.749
Case 2			
$\mathbf{C}_{o,F_o}$	12.215	0	0
(μm/N, μrad/N	0	12.215	0
μm/Nm, μrad/Nm)	0	0	27,335
$\mathbf{C}_{o,F_{in}}$	0.943	0.267	−1.211
(μm/N, μrad/N)	0.853	−1.244	0.390
	−34.159	−34.159	−34.159
$\mathbf{C}_{in,F_{in}}$	0.175	−0.024	−0.024
(μm/N)	−0.024	0.175	−0.024
	−0.024	−0.024	0.175
$\mathbf{J}_{analytical}$	4.749	1.345	−6.093
	4.294	−6.260	1.965
	−266.743	−266.743	−266.743

$$\begin{bmatrix} \mathbf{U_o} \\ \mathbf{U_{in}} \end{bmatrix} = \begin{bmatrix} \mathbf{C_{o,F_o}} & \mathbf{C_{o,F_{in}}} \\ \mathbf{C_{in,F_o}} & \mathbf{C_{in,F_{in}}} \end{bmatrix} \begin{bmatrix} \mathbf{F_o} \\ \mathbf{F_{in}} \end{bmatrix} \quad (1)$$

There are assumptions made throughout the derivation of the kinetostatic model in this paper, which are (a) the structural deformations only occur at flexure hinges and no deformations occur at rigid-linkages, and (b) the translational and rotational displacements are small enough to be linearized. Similar assumptions were also made in other research work to simplify analytical models [18].

The derivation of $\mathbf{C_{o,F_o}}$, $\mathbf{C_{o,F_{in}}}$, $\mathbf{C_{in,F_o}}$ and $\mathbf{C_{in,F_{in}}}$ can be found in Appendix B.

3. Derivation of the closed-form kinematic model

The closed-form kinematics of the 3-RRR micro-motion stage is obtained by calculating the relationship between the input and output displacements using Eq. (1). Assuming there is no external output force acting on the stage, which $\mathbf{F_o} = \mathbf{0}$, Eq. (1) gives,

$$\mathbf{U_o} = \mathbf{C_{o,F_{in}}} \times \mathbf{F_{in}} \quad (2)$$

$$\mathbf{F_{in}} = \mathbf{C_{o,F_{in}}^{-1}} \times \mathbf{U_o} \quad (3)$$

and

$$\mathbf{U_{in}} = \mathbf{C_{in,F_{in}}} \times \mathbf{F_{in}} \quad (4)$$

$$\mathbf{F_{in}} = \mathbf{C_{in,F_{in}}^{-1}} \times \mathbf{U_{in}} \quad (5)$$

By equating Eqs. (3) and (5),

$$\mathbf{U_o} = \mathbf{C_{o,F_{in}}} \times \mathbf{C_{in,F_{in}}^{-1}} \times \mathbf{U_{in}} \quad (6)$$

Table 5
FEA compliance and Jacobian matrices of the SEM micro-motion stage

	FEA results		
$\mathbf{C_{o,F_o}}$	11.498	0	0
(μm/N, μrad/N	0	11.476	0
μm/Nm, μrad/Nm)	0	0	27,966
$\mathbf{C_{o,F_{in}}}$	0.879	0.257	−1.136
(μm/N, μrad/N)	0.803	−1.162	0.357
	−32.141	−32.245	−32.115
$\mathbf{C_{in,F_{in}}}$	0.182	−0.024	−0.024
(μm/N)	−0.024	0.182	−0.024
	−0.024	−0.024	0.182
$\mathbf{J_{FEA}}$	4.259	1.250	−5.499
	3.897	−5.645	1.734
	−240.768	−241.315	−240.481

Table 6
Kinetostatic results of the 3-RRR micro-motion stage and their differences compared to FEA results

	% Diff. compared to FEA					
	Kinetostatic model – Case 1			Kinetostatic model – Case 2		
$\mathbf{C_{o,F_o}}$	−8.8	–	–	6.2	–	–
(μm/N, μrad/N	–	−8.6	–	–	6.4	–
μm/Nm, μrad/Nm)	–	–	−11.5	–	–	−2.3
$\mathbf{C_{o,F_{in}}}$	−7.9	−10.9	−8.5	7.3	3.8	6.6
(μm/N, μrad/N)	−8.8	−8.1	−6.0	6.3	7.1	9.5
	−3.8	−4.1	−3.7	6.3	5.9	6.4
$\mathbf{C_{in,F_{in}}}$	−16.3	−25.5	−25.5	−3.8	−3.7	−3.7
(μm/N)	−25.5	−16.3	−25.5	−3.7	−3.8	−3.7
	−25.5	−25.5	−16.3	−3.7	−3.7	−3.8
$\mathbf{J_{analytical}}$	11.5	7.6	10.8	11.5	7.6	10.8
	10.2	10.9	13.3	10.2	10.9	13.3
	10.8	10.5	10.9	10.8	10.5	10.9

Therefore, the matrix relates the input and output displacements, which is termed the Jacobian matrix **J** in this work, is derived as follows:

$$\mathbf{J} = \mathbf{C}_{\mathbf{o},\mathbf{F}_{\mathbf{in}}} \times \mathbf{C}^{-1}_{\mathbf{in},\mathbf{F}_{\mathbf{in}}} \tag{7}$$

The analytical results of $\mathbf{C}_{\mathbf{o},\mathbf{F}_{\mathbf{o}}}$, $\mathbf{C}_{\mathbf{o},\mathbf{F}_{\mathbf{in}}}$, $\mathbf{C}_{\mathbf{in},\mathbf{F}_{\mathbf{o}}}$, $\mathbf{C}_{\mathbf{in},\mathbf{F}_{\mathbf{in}}}$ and **J** obtained using Eqs. (1) and (7) will be compared to the FEA results in Section 5.

4. Case studies of a 3-RRR compliant micro-motion stage

A 3-RRR compliant micro-motion stage which was designed for the positioning of samples in a scanning-electron-microscope [19] is studied in this paper (see Fig. 12). It is a monolithic compliant mechanism with circular flexure hinges and was manufactured using the wire-electric-discharge-machining (wire-EDM) technique. This stage is actuated by three

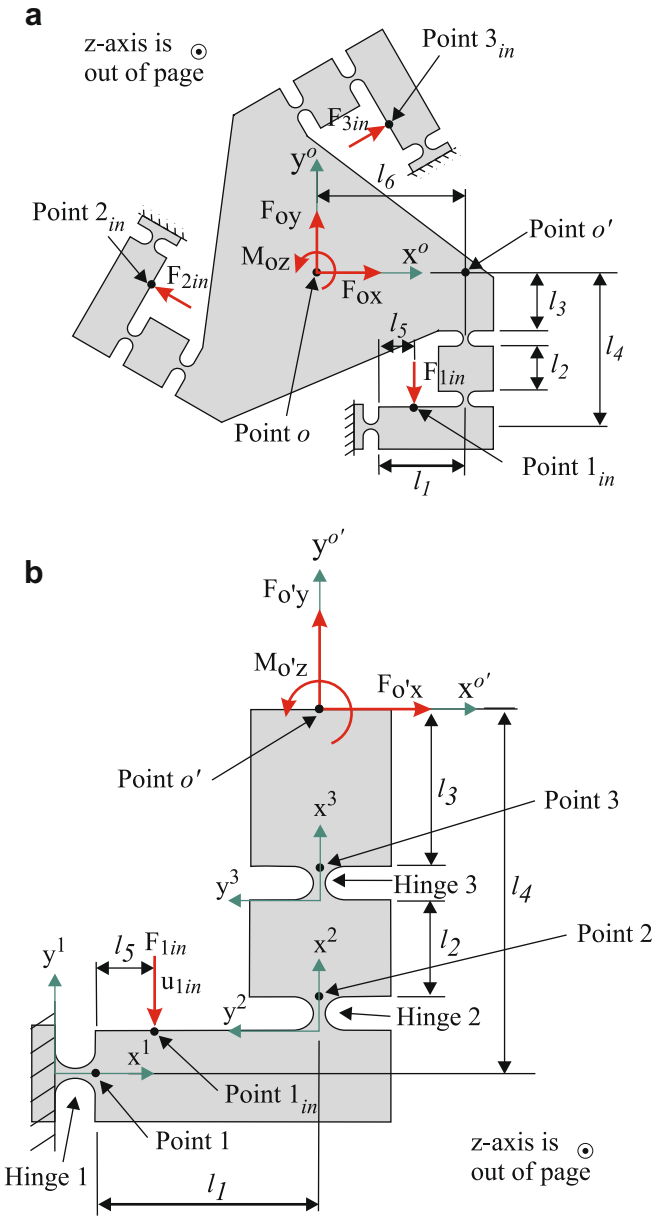

Fig. 6. (a) 3-RRR compliant mechanism. (b) RRR compliant mechanism.

piezo-actuators. It has planar motions along the x and y axes and rotations about the z-axis. The link length, flexure hinge dimensions and material properties of the mechanism are shown in Table 1.

Two cases were studied where analytical matrices of the kinetostatic model of Case 1 were calculated by deliberately choosing the flexure hinge equations which have large differences when compared to the FEA results (refer to Figs. 3–5). Meanwhile, analytical matrices of Case 2 were obtained by choosing the flexure hinge equations which have small differences. Table 2 shows the flexure hinge equations chosen from various published research studies for Case 1 and 2, respectively. Note that for the interests of readers, Table 3 provides a design guideline of choosing a flexure hinge equation for a particular t/R range, and their minimum, maximum and average percentage differences. Related work regarding the development of the guideline can be found in [16]. Table 4 shows the analytical results of Case 1 and 2, respectively.

4.1. Discussion

It can be observed that the off-diagonal terms of compliance matrix, $\mathbf{C}_{\mathbf{o},\mathbf{F_o}}$ are zero. This is expected as the 3-RRR compliant stage has a remote-centre-of-compliance (RCC) configuration and deformations occur only along the direction of the applied force/moment [20]. The 3-RRR stage was designed to have a somewhat decoupled characteristic where the input

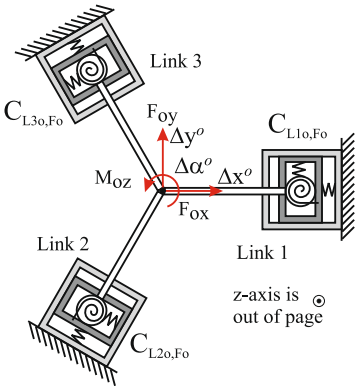

Fig. 7. Parallel spring model of 3-RRR micro-motion stages.

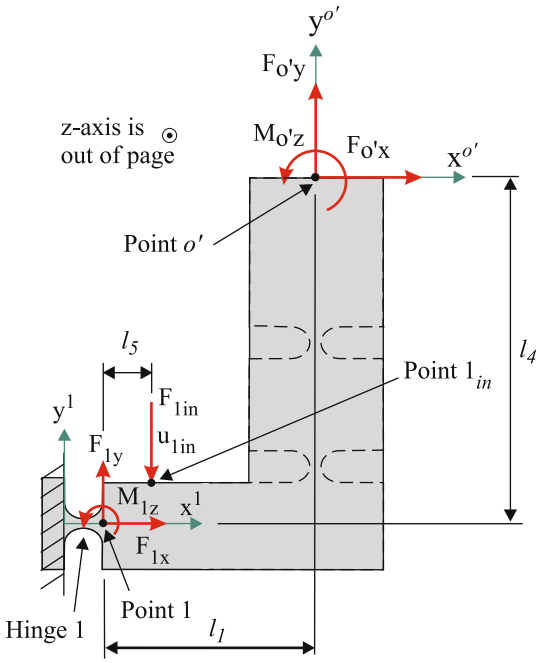

Fig. 8. Compliances due to Hinge 1.

displacements on one link have small effect on the input displacements of the other links. This characteristic can be observed in $\mathbf{C}_{\mathbf{in},\mathbf{F}_{\mathbf{in}}}$. The off-diagonal terms of $\mathbf{C}_{\mathbf{in},\mathbf{F}_{\mathbf{in}}}$ are approximately a factor of 8 smaller than its diagonal terms. It can be observed that the analytical results of Case 1 and 2 are noticeably different except for the Jacobian matrix and the reason will be explained later in this paper. The differences between Case 1 and 2 results suggest that the choice of flexure hinge compliant equations affect the accuracy of the kinetostatic model. Since the kinetostatic model is derived to have flexure hinge compliances as one of the variables, the most suitable flexure hinge equations can be selected by referring to Figs. 3–5 in order to obtain an accurate kinetostatic model. The modeling results of Case 1 and 2 are compared to the FEA results in order to verify their accuracies.

5. Finite-element-analysis (ANSYS)

A two-dimensional FEA model of the 3-RRR compliant stage was generated using ANSYS for comparison purposes. The stage was modeled using 8-node, plane elements (PLANE82) with two-DOF on each node, which are the nodal *x* and *y-directions*. This element type is suitable to model irregular shapes and curved boundaries without much loss of accuracy [21].

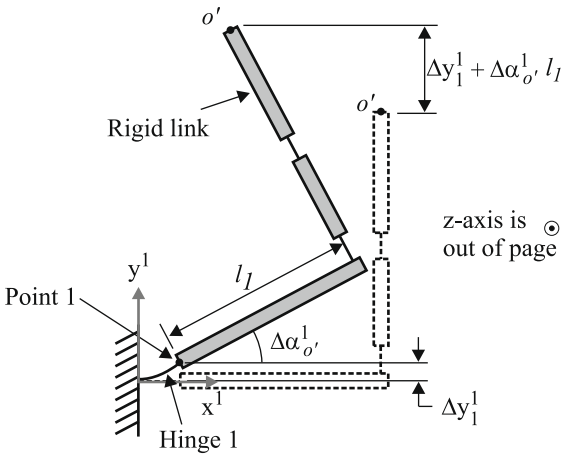

Fig. 9. $\Delta y_{o'}^1$-displacement caused by the amplification of link, l_1. Dashed lines represent initial position of the RRR structure. The flexure hinge is drawn as a solid line and the rigid-link is drawn as a block.

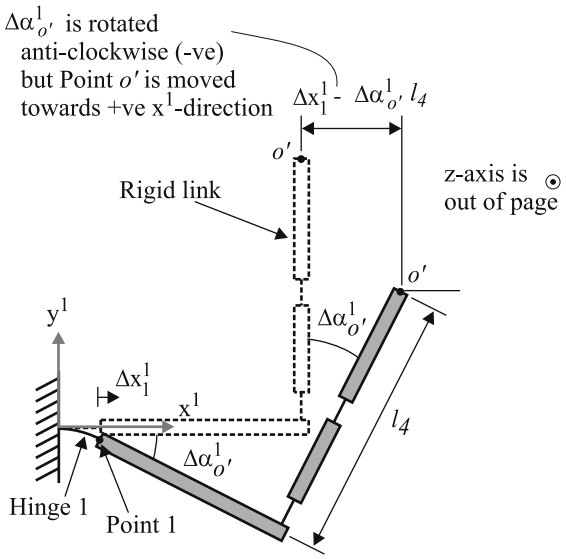

Fig. 10. $\Delta x_{o'}^1$-displacement caused by the amplification of link with distance l_4. Dashed lines represent initial position of the RRR structure. The flexure hinge is drawn as a solid line and the rigid-link is drawn as a block.

The thickness of the model was taken into consideration by using the plane stress element type with thickness option. Plane stress elements were used instead of plain strain elements because plane stress elements provide a safer situation with a possibility of 5–10% underestimation of stiffnesses, while plane strain elements could possibly provide a greater over estimation [14]. To ensure that the mesh size was fine enough, especially near the flexure hinge locations, a number of analyzes were carried out where different mesh sizes were used. The output was checked each time the mesh size was decreased. When a consistent output was obtained, it implied that the mesh was fine enough. When nodal displacements were read from the same node to which forces would be applied, pressures were applied on a line instead to avoid inaccuracy of results associated with singularities on nodes. Meshes and constraints of the FEA model of the 3-RRR micro-motion stage are shown in Fig. 13. The following procedures were carried out to obtain the compliance and Jacobian matrices of the stage:

(1) To obtain the compliance matrix $\mathbf{C}_{\mathbf{o},\mathbf{F_o}}$ of the stage, forces F^*_{ox} and F^*_{oy} were applied at a distance from Point o but along the same lines of action as F_{ox} and F_{oy} (see Fig. 13). The corresponding nodal deformations $(\Delta x_o, \Delta y_o, \Delta\alpha_o)$ at Point o were measured. In order to obtain the compliances corresponding to a unit moment, two equal but opposite forces, F_m were applied as shown. Rotational deformation $(\Delta\alpha_o)$ cannot be measured directly from the node at Point o because the nodes of element type PLANE82 do not have the rotational DOF. However, $\Delta\alpha_o$ can be easily calculated.

(2) To obtain the compliance matrix $\mathbf{C}_{\mathbf{o},\mathbf{F_{in}}}$ of the stage, pressures $(P_{1in}, P_{2in}, P_{3in})$ corresponding to unit input forces were applied on lines where Points 1_{in}, 2_{in} and 3_{in} are located as shown in Fig. 13, and the corresponding nodal deformations $(\Delta x_o, \Delta y_o, \Delta\alpha_o)$ at Point o were measured.

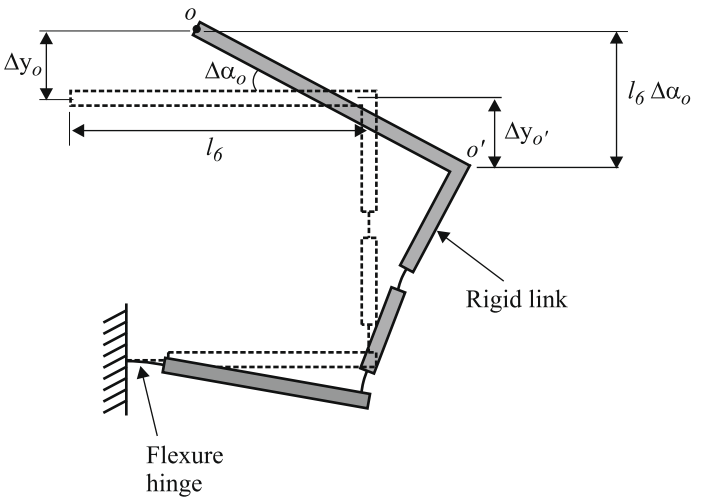

Fig. 11. Calculation of compliances at Point o. Dashed lines represents initial position of the RRR structure. The flexure hinge is drawn as a solid line and the rigid-link is drawn as a block.

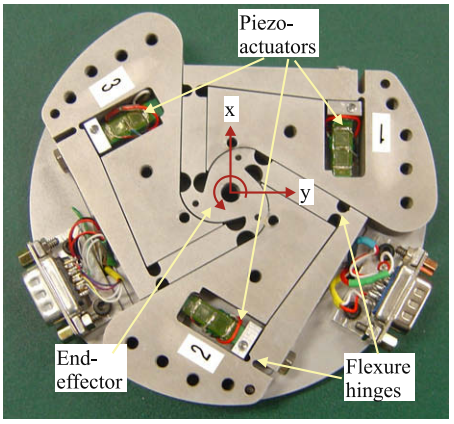

Fig. 12. 3-RRR compliant micro-motion stage.

(3) To obtain the compliance matrix $\mathbf{C}_{\mathbf{in},\mathbf{F_o}}$ of the stage, unit input forces were applied at Point o and the corresponding nodal deformations (u_{1in}, u_{2in}, u_{3in}) at Points 1_{in}, 2_{in} and 3_{in} were measured. Moment was applied using two equal but opposite forces, F_m.
(4) To obtain the compliance matrix $\mathbf{C}_{\mathbf{in},\mathbf{F_{in}}}$ of the stage, pressures (P_{1in}, P_{2in}, P_{3in}) corresponding to unit input forces were applied on lines where Points 1_{in}, 2_{in} and 3_{in} were located, and the corresponding nodal deformations at these points were measured.
(5) To obtain the Jacobian matrix, pressures (P_{1in}, P_{2in}, P_{3in}) were applied independently on lines where Points 1_{in}, 2_{in} and 3_{in} were located. The corresponding input displacements (u_{1in}, u_{2in}, u_{3in}) at Points 1_{in}, 2_{in} and 3_{in}, and the output displacement (Δx_o, Δy_o, $\Delta\alpha_o$) at Point o were measured. The Jacobian matrix was obtained where the output displacements were divided by the input displacements.

Table 5 shows the results of the compliance and Jacobian matrices of the micro-motion stage. $\mathbf{C}_{\mathbf{in},\mathbf{F_o}}$ is the transpose of $\mathbf{C}_{\mathbf{o},\mathbf{F_{in}}}$. Therefore, the results of $\mathbf{C}_{\mathbf{in},\mathbf{F_o}}$ are not repeated in Table 5.

5.1. Comparison of analytical results with FEA

The results of kinetostatic models of Case 1 and 2 obtained in Section 2 were compared to the FEA results. Table 6 shows the differences of the kinetostatic results when compared to that of the FEA.

5.1.1. Discussion

By comparing the kinetostatic results of Case 1 and 2 of the 3-RRR compliant micro-motion stage to the FEA results, it can be noted that the differences of the output ($\mathbf{C}_{\mathbf{o},\mathbf{F_o}}$) and input ($\mathbf{C}_{\mathbf{in},\mathbf{F_{in}}}$) compliance matrices are significantly reduced for Case 2. The choice of flexure hinge compliance equations, in these case studies, only slightly varies the accuracy of $\mathbf{C}_{\mathbf{o},\mathbf{F_{in}}}$. The same is true for the Jacobian matrices of Cases 1 and 2. This is because the Jacobian matrix represents the kinematics of the

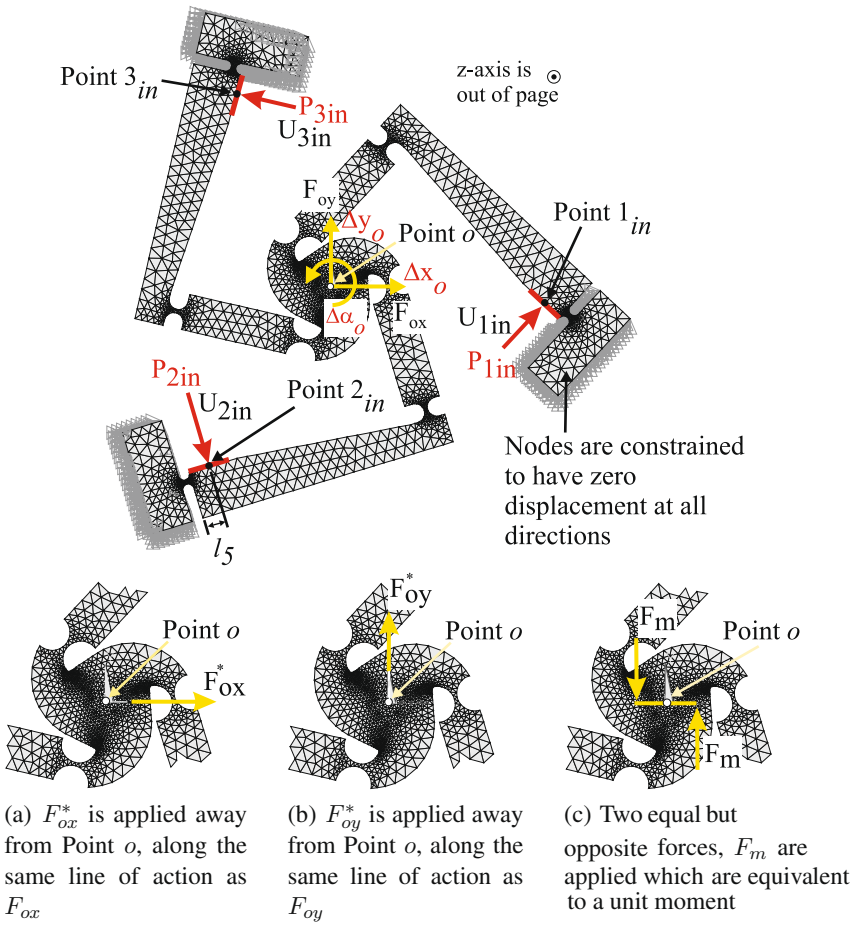

Fig. 13. FEA model of the 3-RRR compliant micro-motion stage.

micro-motion structures, and therefore it is independent to the compliances or stiffnesses of flexure hinges. The choice of flexure hinge equations used to calculate the analytical results has minimal effect on the results of the Jacobian matrix. Nevertheless, the compliance results of $\mathbf{C}_{\mathbf{o},\mathbf{F_o}}$ and $\mathbf{C}_{\mathbf{in},\mathbf{F_{in}}}$ are improved significantly when the suitable flexure hinge equations are used (Case 2).

The derived kinetostatic model in this paper is capable of providing good predictions of the kinematics, and both the input and output compliances when compared to the FEA results. The kinetostatic model in Case 2 predicts (a) the kinematics of the 3-RRR mechanism to be within 13%, (b) the input compliances to be within 4%, and (c) the output compliances to be within 6% when compared to the FEA results. These differences could be attributed to the assumption made in deriving the kinetostatic model. The kinetostatic model assumes that the deformation of rigid-links of the micro-motion stage is small and can be ignored. This assumption is made because the 3-RRR compliant structure is not an over-constrained structure. Therefore, deformations are not expected at rigid-links [22]. However, the small differences between the kinetostatic results and the FEA results could be due to these unmodeled rigid-link deformations. The differences between the kinetostatic and the FEA results could also be attributed to the errors of the flexure hinge compliance equations chosen (see Figs. 3–5). Although flexure hinge compliance equations which have small differences when compared to FEA results were chosen in Case 2, these small differences could be enlarged through linkages of the 3-RRR compliant structure.

6. Conclusions

A kinetostatic model of a 3-RRR compliant micro-motion stage, which allows the fulfillment of both the kinematics and the force design criteria of compliant micro-motion stages, is derived and presented in this paper. The derived kinetostatic model in this paper can be used to predict the kinematics, and both the input and output compliances/stiffnesses of 3-RRR compliant mechanisms. The kinetostatic model has closed-form equations, and circular flexure hinge compliances are one of the variables in the model. Therefore, researchers can choose the most suitable flexure hinge compliance equations in order to calculate the kinetostatics of compliant stages accurately. Two cases of the kinetostatic results of a 3-RRR compliant mechanism were studied in this paper. The kinetostatic results of Case 1 were calculated by deliberately choosing the flexure hinge equations which have large differences when compared to FEA results. Meanwhile, the kinetostatic results of Case 2 were calculated by choosing the flexure hinge equations which have small differences. It can be observed that the kinetostatic results of Case 1 and 2 were noticeably different. These results suggest that the choice of flexure hinge compliance equations affects the accuracy of the kinetostatic model of the 3-RRR mechanism. The modeling results of Case 1 and 2 were compared to the FEA results in order to verify their accuracy. The comparisons show that the differences of the output and input compliances ($\mathbf{C}_{\mathbf{o},\mathbf{F_o}}$ and $\mathbf{C}_{\mathbf{in},\mathbf{F_{in}}}$) were reduced significantly for Case 2. The differences of Jacobian matrices of Case 1 and 2 were the same. Jacobian matrices represent the kinematics of the micro-motion structures, and the choice of flexure hinge equations used to calculate the analytical results has minimal effect on the results of the Jacobian matrix.

The derived kinetostatic model was capable of providing good predictions of the kinematics (within 13%), and both the input (within 4%) and output (within 6%) compliances when compared to the FEA results. The accuracy of the kinetostatic model will be experimentally verified in near future.

Acknowledgements

The authors would like to greatly acknowledge the support of the Adelaide Robotics Research Group at the University of Adelaide and the use of its facilities. The authors would also like to acknowledge the instrumentation and workshop staff at the School of Mechanical Engineering for all their help. Also, a special thanks to George Osborne for his innovative ideas and excellent craftsmanship.

Appendix A. Nomenclature

Nomenclature	Note: Vectors and matrices are shown in bold face.
Subscripts	
1, 2, 3, *o′*, *o*	Point 1, 2, 3, o′, o
x, *y*, *z*	reference axes
*h*1, *h*2, *h*3	Hinge 1, 2, 3
L_1, L_2, L_3	Links 1, 2, 3
Superscript	
1, 2, 3	reference axes of flexure hinges
Symbols	
x, y	reference axes
Δx, Δy	translational displacements in the *x*-, *y*-axis, also named as Δx-displacement and Δy-displacement
$\Delta\alpha$	rotational displacements along the *z*-axis, also named as $\Delta\alpha$-displacement

Appendix A (*continued*)

Nomenclature	Note: Vectors and matrices are shown in bold face.
C	compliance matrix
F, M	forces, moment
$\partial\Delta x/\partial F$, $\partial\Delta x/\partial M$	the change of Δx-displacement due to forces/moments (compliance)
$\partial\Delta y/\partial F$, $\partial\Delta y/\partial M$	the change of Δy-displacement due to forces/moments (compliance)
$\partial\Delta\alpha/\partial F$, $\partial\Delta\alpha/\partial M$	the change of $\Delta\alpha$-displacement due to forces/moments (compliance)
$[\alpha_z/M_z]_j$,$[\Delta y/F_y]_j$, $[\Delta x/F_x]_j$	compliances of flexure hinge j, where $j = 1,2,3$
t_j	smallest thickness of flexure hinge j, where $j = 1,2,3$
R_j	radius of flexure hinge j, where $j = 1,2,3$
$\mathbf{U_o}$	3×1 matrix representing the output displacements $(\Delta x_o, \Delta y_o, \Delta\alpha_o)$ of the stage
$\mathbf{U_{in}}$	3×1 matrix representing the input displacements $(u_{1\text{in}},\ u_{2\text{in}},\ u_{3\text{in}})$ of the stage. The input displacements are along the direction of the input forces
$\mathbf{F_o}$	3×1 matrix representing the output forces/moments acting at Point o (F_{ox}, F_{oy}, M_{oz})
$\mathbf{F_{in}}$	3×1 matrix representing the input forces $(F_{1\text{in}}, F_{2\text{in}}, F_{3\text{in}})$
$\mathbf{C_{o,F_o}}$	3×3 compliance matrix relating the output displacements to the output forces/moments
$\mathbf{C_{o,F_{in}}}$	3×3 compliance matrix relating the output displacements to the input forces
$\mathbf{C_{in,F_o}}$	3×3 compliance matrix relating the input displacements to the output forces/moments
$\mathbf{C_{in,F_{in}}}$	3×3 compliance matrix relating the input displacements to the input forces
D	displacement matrix

Appendix B. Derivation of output compliance matrix, $\mathbf{C}_{o,F_o}$

The schematic of a 3-RRR compliant micro-motion stage is shown in Fig. 6. Due to the symmetrical structure of the 3-RRR compliant micro-motion stage, the 3-RRR structure can be divided into three links in order to calculate the $\mathbf{C_{o,F_o}}$ matrix. Each link consists of a RRR topology which has three circular flexure hinges. The flexure hinge compliances are $[\Delta\alpha_z/M_z]_j$, $[\Delta y/F_y]_j$ and $[\Delta x/F_x]_j$, where $j = 1,2,3$. The RRR compliant structure is shown in Fig. 6b together with its dimensions, displacements, local coordinates of flexure hinges and the applied forces/moments. The compliances at Point $o\prime$ contributed by each flexure hinge in the structure are firstly calculated. These compliance matrices are named $\mathbf{C_{h1}}$, $\mathbf{C_{h2}}$ and $\mathbf{C_{h3}}$. The three flexure hinges of the RRR structure are arranged in series; therefore the compliance matrix of the RRR structure at Point $o\prime$ can be obtained by summing $\mathbf{C_{h1}}$, $\mathbf{C_{h2}}$ and $\mathbf{C_{h3}}$. The compliance matrices of the three RRR links are referred to as $\mathbf{C_{L_1o,F_o}}$, $\mathbf{C_{L_2o,F_o}}$ and $\mathbf{C_{L_3o,F_o}}$, respectively. The three RRR links of the 3-RRR compliant structure are arranged in parallel; therefore $\mathbf{C_{o,F_o}}$ matrix in Eq. (1) is calculated by summing $\mathbf{C_{L_1o,F_o}}$, $\mathbf{C_{L_2o,F_o}}$ and $\mathbf{C_{L_3o,F_o}}$ using the rule of parallel connection of springs (see Fig. 7).

B.1. Compliances of the RRR mechanism due to Hinge 1

The compliance matrix of the RRR mechanism due to Hinge 1 is expressed as,

$$\mathbf{C_{h1}} = \begin{bmatrix} \partial\Delta x^1_{o\prime}/\partial F_{o\prime x} & \partial\Delta x^1_{o\prime}/\partial F_{o\prime y} & \partial\Delta x^1_{o\prime}/\partial M_{o\prime z} \\ \partial\Delta y^1_{o\prime}/\partial F_{o\prime x} & \partial\Delta y^1_{o\prime}/\partial F_{o\prime y} & \partial\Delta y^1_{o\prime}/\partial M_{o\prime z} \\ \partial\Delta\alpha^1_{o\prime}/\partial F_{o\prime x} & \partial\Delta\alpha^1_{o\prime}/\partial F_{o\prime y} & \partial\Delta\alpha^1_{o\prime}/\partial M_{o\prime z} \end{bmatrix} \tag{B.8}$$

where the partial derivative terms in Eq. (B.8) are derived as follows:

B.1.1. Derivation of $\partial\Delta\alpha^1_{o\prime}/\partial F_{o\prime x}$, $\partial\Delta\alpha^1_{o\prime}/\partial F_{o\prime y}$ and $\partial\Delta\alpha^1_{o\prime}/\partial M_{o\prime z}$

From Fig. 8, forces/moments acting at Point $o\prime$ and Point 1_{in} can be resolved into forces/moments acting at Point 1 as shown below,

$$F_{1x} = F_{o\prime x}$$
$$F_{1y} = F_{o\prime y} - F_{1\text{in}}$$
$$M_{1z} = -F_{o\prime x}l_4 + F_{o\prime y}l_1 + M_{o\prime z} - F_{1\text{in}}l_5$$

The rotational displacements along the z-axis, $\Delta\alpha^1_1$ at Point 1 can be calculated as shown below,

$$\begin{aligned} \Delta\alpha^1_1 &= \left[\frac{\Delta\alpha_z}{M_z}\right]_1 M_{1z} + \left[\frac{\Delta\alpha_z}{M_z}\right]_1 F_{1y}R_1 \\ &= \left[\frac{\Delta\alpha_z}{M_z}\right]_1 \{-F_{o\prime x}l_4 + F_{o\prime y}(l_1 + R_1) + M_{o\prime z} - F_{1\text{in}}(l_5 + R_1)\} \end{aligned} \tag{B.9}$$

The $\Delta\alpha^1_1$-compliances of Hinge 1 caused by $F_{o\prime x}$, $F_{o\prime y}$ and $M_{o\prime z}$ are obtained by taking the partial derivatives of $\Delta\alpha^1_1$ with respect to the forces/moments acting at Point $o\prime$,

$$\frac{\partial \Delta\alpha_1^1}{\partial F_{o'x}} = -l_4\left[\frac{\Delta\alpha_z}{M_z}\right]_1 \tag{B.10}$$

$$\frac{\partial \Delta\alpha_1^1}{\partial F_{o'y}} = (l_1 + R_1)\left[\frac{\Delta\alpha_z}{M_z}\right]_1 \tag{B.11}$$

$$\frac{\partial \Delta\alpha_1^1}{\partial M_{o'z}} = \left[\frac{\Delta\alpha_z}{M_z}\right]_1 \tag{B.12}$$

The results of the partial derivatives of $\Delta\alpha_1^1$ in Eqs. (B.10), (B.11) and (B.12) describe the relationship between the $\Delta\alpha_1^1$-displacement and the forces/moments.

The $\Delta\alpha_{o'}^1$-displacement at Point $o\prime$ is the same as the $\Delta\alpha_1^1$-displacement at Point 1. Therefore, $\partial\Delta\alpha_{o'}^1/\partial F_{o'x}$, $\partial\Delta\alpha_{o'}^1/\partial F_{o'y}$ and $\partial\Delta\alpha_{o'}^1/\partial M_{o'z}$ are the same as Eqs. (B.10), (B.11) and (B.12).

B.1.2. Derivation of $\partial\Delta y_{o'}^1/\partial F_{o'x}$, $\partial\Delta y_{o'}^1/\partial F_{o'y}$ and $\partial\Delta y_{o'}^1/\partial M_{o'z}$

The translational displacements along the y-axis, Δy_1^1 at Point 1 can be calculated as shown below,

$$\Delta y_1^1 = \left[\frac{\Delta y}{F_y}\right]_1 F_{1y} + \left[\frac{\Delta\alpha_z}{M_z}\right]_1 M_{1z}R_1 = \left[\frac{\Delta y}{F_y}\right]_1 (F_{o'y} - F_{1\text{in}}) + \left[\frac{\Delta\alpha_z}{M_z}\right]_1 (-F_{o'x}l_4 + F_{o'y}l_1 + M_{o'z} - F_{1\text{in}}l_5)R_1 \tag{B.13}$$

The Δy_1^1-compliances of Hinge 1 caused by $F_{o'x}$, $F_{o'y}$ and $M_{o'z}$ are obtained by taking the partial derivatives of Δy_1^1 with respect to the forces/moments acting at Point o',

$$\frac{\partial \Delta y_1^1}{\partial F_{o'x}} = -l_4R_1\left[\frac{\Delta\alpha_z}{M_z}\right]_1 \tag{B.14}$$

$$\frac{\partial \Delta y_1^1}{\partial F_{o'y}} = \left[\frac{\Delta y}{F_y}\right]_1 + l_1R_1\left[\frac{\Delta\alpha_z}{M_z}\right]_1 \tag{B.15}$$

$$\frac{\partial \Delta y_1^1}{\partial M_{o'z}} = R_1\left[\frac{\Delta\alpha_z}{M_z}\right]_1 \tag{B.16}$$

Due to the amplification of the link with distance l_1, the translational displacement along the y-axis, $\Delta y_{o'}^1$ at Point $o\prime$ is the summation of Δy_1^1-displacement at Point 1 and the amplified displacements caused by the rotational motions of the link (see Fig. 9). Therefore, the $\Delta y_{o'}^1$-displacement is,

$$\Delta y_{o'}^1 = \Delta y_1^1 + \Delta\alpha_{o'}^1 l_1 \tag{B.17}$$

The $\Delta y_{o'}^1$-compliances of Hinge 1 caused by $F_{o'x}$, $F_{o'y}$ and $M_{o'z}$ are obtained by taking the partial derivatives of $\Delta y_{o'}^1$ with respect to all the forces/moments acting at Point o',

$$\frac{\partial \Delta y_{o'}^1}{\partial F_{o'x}} = \frac{\partial \Delta y_1^1}{\partial F_{o'x}} + \frac{\partial \Delta\alpha_{o'}^1}{\partial F_{o'x}} l_1 = -l_4(l_1 + R_1)\left[\frac{\Delta\alpha_z}{M_z}\right]_1 \tag{B.18}$$

$$\frac{\partial \Delta y_{o'}^1}{\partial F_{o'y}} = \frac{\partial \Delta y_1^1}{\partial F_{o'y}} + \frac{\partial \Delta\alpha_{o'}^1}{\partial F_{o'y}} l_1 = \left[\frac{\Delta y}{F_y}\right]_1 + \{l_1R_1 + l_1(l_1 + R_1)\}\left[\frac{\Delta\alpha_z}{M_z}\right]_1 \tag{B.19}$$

$$\frac{\partial \Delta y_{o'}^1}{\partial M_{o'z}} = \frac{\partial \Delta y_1^1}{\partial M_{o'z}} + \frac{\partial \Delta\alpha_{o'}^1}{\partial M_{o'z}} l_1 = (l_1 + R_1)\left[\frac{\Delta\alpha_z}{M_z}\right]_1 \tag{B.20}$$

B.1.3. Derivation of $\partial\Delta x_{o'}^1/\partial F_{o'x}$, $\partial\Delta x_{o'}^1/\partial F_{o'y}$ and $\partial\Delta x_{o'}^1/\partial M_{o'z}$

The translational displacements along the x-axis, Δx_1^1 at Point 1 can be calculated as shown below,

$$\begin{aligned}\Delta x_1^1 &= \left[\frac{\Delta x}{F_x}\right]_1 F_{1x} \\ &= \left[\frac{\Delta x}{F_x}\right]_1 F_{o'x}\end{aligned} \tag{B.21}$$

The Δx_1^1-compliances of Hinge 1 caused by $F_{o'x}$, $F_{o'y}$ and $M_{o'z}$ are obtained by taking the partial derivatives of Δx_1^1 with respect to the forces/moments acting at Point o',

$$\frac{\partial \Delta x_1^1}{\partial F_{o'x}} = \left[\frac{\Delta x}{F_x}\right]_1 \tag{B.22}$$

$$\frac{\partial \Delta x_1^1}{\partial F_{o'y}} = 0 \tag{B.23}$$

$$\frac{\partial \Delta x_1^1}{\partial M_{o'z}} = 0 \tag{B.24}$$

Due to the amplification of the link with distance l_4, the translational displacements along the x-axis, $\Delta x^1_{o'}$ at Point o is the summation of Δx^1_1-displacement at Point 1 and the amplified displacements caused by the rotational motions of the link (see Fig. 10). Therefore, the $\Delta x^1_{o'}$-displacement is,

$$\Delta x^1_{o'} = \Delta x^1_1 - \Delta\alpha^1_{o'} l_4 \tag{B.25}$$

The negative sign of $\Delta\alpha^1_{o'} l_4$ is due to the fact that when $\Delta\alpha^1_{o'}$ is rotated towards the anti-clockwise direction (negative rotations), Point $o\prime$ is moved towards the positive Δx^1-direction.

The $\Delta x^1_{o'}$-compliances of Hinge 1 caused by $F_{o'x}$, $F_{o'y}$ and $M_{o'z}$ are obtained by taking the partial derivatives of $\Delta x^1_{o'}$ with respect to the forces/moments acting at Point o',

$$\frac{\partial\Delta x^1_{o'}}{\partial F_{o'x}} = \frac{\partial\Delta x^1_1}{\partial F_{o'x}} - \frac{\partial\Delta\alpha^1_{o'}}{\partial F_{o'x}} l_4 = \left[\frac{\Delta x}{F_x}\right]_1 + l_4^2\left[\frac{\Delta\alpha_z}{M_z}\right]_1 \tag{B.26}$$

$$\frac{\partial\Delta x^1_{o'}}{\partial F_{o'y}} = \frac{\partial\Delta x^1_1}{\partial F_{o'y}} - \frac{\partial\Delta\alpha^1_{o'}}{\partial F_{o'y}} l_4 = -l_4(l_1 + R_1)\left[\frac{\Delta\alpha_z}{M_z}\right]_1 \tag{B.27}$$

$$\frac{\partial\Delta x^1_{o'}}{\partial M_{o'z}} = \frac{\partial\Delta x^1_1}{\partial M_{o'z}} - \frac{\partial\Delta\alpha^1_{o'}}{\partial M_{o'z}} l_4 = -l_4\left[\frac{\Delta\alpha_z}{M_z}\right]_1 \tag{B.28}$$

By substituting Eqs. (B.10)–(B.12), (B.18)–(B.20) and (B.26)–(B.28) into Eq. (B.8), the compliance matrix of the RRR structure due to Hinge 1, $\mathbf{C_{h1}}$ can be obtained.

Similar method is used to derive $\mathbf{C_{h2}}$ and $\mathbf{C_{h3}}$.

B.2. Compliances of the RRR mechanism due to Hinge 2

The compliance matrix of the RRR structure due to Hinge 2 is expressed as,

$$\mathbf{C_{h2}} = \begin{bmatrix} \partial\Delta x^2_{o'}/\partial F_{o'x} & \partial\Delta x^2_{o'}/\partial F_{o'y} & \partial\Delta x^2_{o'}/\partial M_{o'z} \\ \partial\Delta y^2_{o'}/\partial F_{o'x} & \partial\Delta y^2_{o'}/\partial F_{o'y} & \partial\Delta y^2_{o'}/\partial M_{o'z} \\ \partial\Delta\alpha^2_{o'}/\partial F_{o'x} & \partial\Delta\alpha^2_{o'}/\partial F_{o'y} & \partial\Delta\alpha^2_{o'}/\partial M_{o'z} \end{bmatrix} \tag{B.29}$$

where the partial derivative terms in Eq. (B.29) are shown as follows:

$$\frac{\partial\Delta\alpha^2_{o'}}{\partial F_{o'x}} = -(l_2 + l_3 + 2R_3 + R_2)\left[\frac{\Delta\alpha_z}{M_z}\right]_2 \tag{B.30}$$

$$\frac{\partial\Delta\alpha^2_{o'}}{\partial F_{o'y}} = 0 \tag{B.31}$$

$$\frac{\partial\Delta\alpha^2_{o'}}{\partial M_{o'z}} = \left[\frac{\Delta\alpha_z}{M_z}\right]_2 \tag{B.32}$$

$$\frac{\partial\Delta y^2_{o'}}{\partial F_{o'x}} = \frac{\partial\Delta y^2_2}{\partial F_{o'x}} + \frac{\partial\Delta\alpha^2_{o'}}{\partial F_{o'x}}(l_2 + l_3 + 2R_3) = -\left[\frac{\Delta y}{F_y}\right]_2 - \{(l_2 + l_3 + 2R_3)R_2 + (l_2 + l_3 + 2R_3)(l_2 + l_3 + 2R_3 + R_2)\}\left[\frac{\Delta\alpha_z}{M_z}\right]_2 \tag{B.33}$$

$$\frac{\partial\Delta y^2_{o'}}{\partial F_{o'y}} = \frac{\partial\Delta y^2_2}{\partial F_{o'y}} + \frac{\partial\Delta\alpha^2_{o'}}{\partial F_{o'y}}(l_2 + l_3 + 2R_3) = 0 \tag{B.34}$$

$$\frac{\partial\Delta y^2_{o'}}{\partial M_{o'z}} = \frac{\partial\Delta y^2_2}{\partial M_{o'z}} + \frac{\partial\Delta\alpha^2_{o'}}{\partial M_{o'z}}(l_2 + l_3 + 2R_3) = (l_2 + l_3 + R_2 + 2R_3)\left[\frac{\Delta\alpha_z}{M_z}\right]_2 \tag{B.35}$$

$$\frac{\partial\Delta x^2_2}{\partial F_{o'x}} = 0 \tag{B.36}$$

$$\frac{\partial\Delta x^2_2}{\partial F_{o'y}} = \left[\frac{\Delta x}{F_x}\right]_2 \tag{B.37}$$

$$\frac{\partial\Delta x^2_2}{\partial M_{o'z}} = 0 \tag{B.38}$$

B.3. Compliances of the RRR mechanism due to Hinge 3

The compliance matrix of the RRR structure due to Hinge 3 is expressed as,

$$\mathbf{C_{h3}} = \begin{bmatrix} \partial\Delta x^3_{o'}/\partial F_{o'x} & \partial\Delta x^3_{o'}/\partial F_{o'y} & \partial\Delta x^3_{o'}/\partial M_{o'z} \\ \partial\Delta y^3_{o'}/\partial F_{o'x} & \partial\Delta y^3_{o'}/\partial F_{o'y} & \partial\Delta y^3_{o'}/\partial M_{o'z} \\ \partial\Delta\alpha^3_{o'}/\partial F_{o'x} & \partial\Delta\alpha^3_{o'}/\partial F_{o'y} & \partial\Delta\alpha^3_{o'}/\partial M_{o'z} \end{bmatrix} \tag{B.39}$$

where the partial derivative terms in Eq. (B.39) are shown as follows:

$$\frac{\partial \Delta\alpha^3_{o'}}{\partial F_{o'x}} = -(l_3 + R_3)\left[\frac{\Delta\alpha_z}{M_z}\right]_3 \tag{B.40}$$

$$\frac{\partial \Delta\alpha^3_{o'}}{\partial F_{o'y}} = 0 \tag{B.41}$$

$$\frac{\partial \Delta\alpha^3_{o'}}{\partial M_{o'z}} = \left[\frac{\Delta\alpha_z}{M_z}\right]_3 \tag{B.42}$$

$$\frac{\partial \Delta y^3_{o'}}{\partial F_{o'x}} = \frac{\partial \Delta y^3_3}{\partial F_{o'x}} + \frac{\partial \Delta\alpha^3_{o'}}{\partial F_{o'x}} l_3 = -\left[\frac{\Delta y}{F_y}\right]_3 - l_3(l_3 + 2R_3)\left[\frac{\Delta\alpha_z}{M_z}\right]_3 \tag{B.43}$$

$$\frac{\partial \Delta y^3_{o'}}{\partial F_{o'y}} = \frac{\partial \Delta y^3_3}{\partial F_{o'y}} + \frac{\partial \Delta\alpha^3_{o'}}{\partial F_{o'y}} l_3 = 0 \tag{B.44}$$

$$\frac{\partial \Delta y^3_{o'}}{\partial M_{o'z}} = \frac{\partial \Delta y^3_3}{\partial M_{o'z}} + \frac{\partial \Delta\alpha^3_{o'}}{\partial M_{o'z}} l_3 = (l_3 + R_3)\left[\frac{\Delta\alpha_z}{M_z}\right]_3 \tag{B.45}$$

$$\frac{\partial \Delta x^3_{o'}}{\partial F_{o'x}} = 0 \tag{B.46}$$

$$\frac{\partial \Delta x^3_{o'}}{\partial F_{o'y}} = \left[\frac{\Delta x}{F_x}\right]_3 \tag{B.47}$$

$$\frac{\partial \Delta x^3_{o'}}{\partial M_{o'z}} = 0 \tag{B.48}$$

B.4. Compliance matrices of Links 1, 2 and 3

Since the three flexure hinges are arranged in series in the RRR structure, the overall compliances of the RRR structure at Point o' can be calculated by summing the compliance matrices, $\mathbf{C_{h1}}$, $\mathbf{C_{h2}}$ and $\mathbf{C_{h3}}$. However, the compliance matrices $\mathbf{C_{h2}}$ and $\mathbf{C_{h3}}$ are defined using the local coordinate of x^2y^2, and x^3y^3, respectively. These local coordinates are orientated 90° from the coordinate of $x^{o'}y^{o'}$. Therefore, $\mathbf{C_{h2}}$ and $\mathbf{C_{h3}}$ need to be rotated by 90° before the summation. The rotated $\mathbf{C_{h2}}$ and $\mathbf{C_{h3}}$ are referred to as $\mathbf{C'_{h2}}$ and $\mathbf{C'_{h3}}$, respectively.

$$\mathbf{C'_{h2}} = \mathbf{T_{\pi/2}} \times \mathbf{C_{h2}} \tag{B.49}$$

$$\mathbf{C'_{h3}} = \mathbf{T_{\pi/2}} \times \mathbf{C_{h3}} \tag{B.50}$$

where

$$\mathbf{T_{\pi/2}} = \begin{bmatrix} \cos(\pi/2) & -\sin(\pi/2) & 0 \\ \sin(\pi/2) & \cos(\pi/2) & 0 \\ 0 & 0 & 1 \end{bmatrix} \tag{B.51}$$

The compliance matrix at Point $o\prime$ of Link 1, which is the first RRR link in the 3-RRR micro-motion structure is,

$$\mathbf{C_{L_1 o', F_{o'}}} = \mathbf{C_{h1}} + \mathbf{C'_{h2}} + \mathbf{C'_{h3}} \tag{B.52}$$

where the subscript "L_1" indicates Link 1 of the 3-RRR structure.

The output displacements at Point $o\prime$ of Link 1 is,

$$\begin{bmatrix} \Delta x_{o'} \\ \Delta y_{o'} \\ \alpha_{o'} \end{bmatrix}_{L_1} = \mathbf{C_{L_1 o', F_{o'}}} \times \mathbf{F_{o'}} \tag{B.53}$$

where $\mathbf{F_{o'}} = [F_{o'x} \quad F_{o'y} \quad M_{o'z}]^{\mathrm{T}}$.

When output forces are applied at Point o instead of Point $o\prime$ (see Fig. 6a) and the displacements at this point are desired, matrix T_f can be used to transfer the output forces from Point o to Point $o\prime$. Once $\mathbf{C_{L_1 o', F_{o'}}}$ is determined using Eq. (B.52), the compliances at Point o can be calculated by transforming $\mathbf{C_{L_1 o', F_{o'}}}$ to Point o using a matrix, $\mathbf{T_d}$. Intuitively, we know that $\Delta x_o = \Delta x_{o'}$ and $\Delta\alpha_o = \Delta\alpha_{o'}$. However, $\Delta y_o \neq \Delta y_{o'}$ due to rotational motions ($\Delta\alpha_{o'}$) and the amplification of lever arm, l_6. This link amplification effect is taken into consideration by the matrix $\mathbf{T_d}$. Displacement Δy_o of the RRR stage is illustrated in Figs. 11 and 13.

The force transformation matrix is,

$$\mathbf{T_f} = \begin{bmatrix} 1 & 0 & 0 \\ 0 & 1 & 0 \\ 0 & -l_6 & 1 \end{bmatrix} \tag{B.54}$$

where

$$\mathbf{F_{o'}} = \mathbf{T_f} \times \mathbf{F_o} \tag{B.55}$$

and

$$\mathbf{F_o} = [F_{ox} \quad F_{oy} \quad M_{oz}]^{\mathrm{T}}$$

The displacement transformation matrix is,

$$\mathbf{T_d} = \begin{bmatrix} 1 & 0 & 0 \\ 0 & 1 & -l_6 \\ 0 & 0 & 1 \end{bmatrix} \tag{B.56}$$

The output displacements at Point o of Link 1 is,

$$\begin{bmatrix} \Delta x_o \\ \Delta y_o \\ \Delta \alpha_o \end{bmatrix}_{L_1} = \mathbf{T_d} \times \mathbf{C_{L_1 o', F_{o'}}} \times (\mathbf{T_f} \times \mathbf{F_o}) \tag{B.57}$$

Therefore, the compliance of Link 1 at Point o is,

$$\mathbf{C_{L_1 o, F_o}} = \mathbf{T_d} \times \mathbf{C_{L_1 o', F_{o'}}} \times \mathbf{T_f} \tag{B.58}$$

Since Link 2 and Link 3 are arranged to be -120° and 120° apart from Link 1, the compliance of Link 2 and Link 3 at Point o can be obtained as shown below.

The displacements, $\mathbf{D_{L_2 o, F_o}}$ and $\mathbf{D_{L_3 o, F_o}}$ at Point o due to compliances of Links 2 and 3, respectively are,

$$\mathbf{D_{L_2 o, F_o}} = \mathbf{T_{-2\pi/3}} \times \mathbf{C_{L_1 o, F_o}} \times \mathbf{T^{T}_{-2\pi/3}} \times \mathbf{F_o} \tag{B.59}$$

$$\mathbf{D_{L_3 o, F_o}} = \mathbf{T_{2\pi/3}} \times \mathbf{C_{L_1 o, F_o}} \times \mathbf{T^{T}_{2\pi/3}} \times \mathbf{F_o} \tag{B.60}$$

where

$$\mathbf{T_{2\pi/3}} = \begin{bmatrix} \cos(2\pi/3) & -\sin(2\pi/3) & 0 \\ \sin(2\pi/3) & \cos(2\pi/3) & 0 \\ 0 & 0 & 1 \end{bmatrix} \tag{B.61}$$

$$\mathbf{T_{-2\pi/3}} = \begin{bmatrix} \cos(-2\pi/3) & -\sin(-2\pi/3) & 0 \\ \sin(-2\pi/3) & \cos(-2\pi/3) & 0 \\ 0 & 0 & 1 \end{bmatrix} \tag{B.62}$$

and $\mathbf{T^{T}_{2\pi/3}}$ and $\mathbf{T^{T}_{-2\pi/3}}$ are the transpose of $\mathbf{T_{2\pi/3}}$ and $\mathbf{T_{-2\pi/3}}$, respectively.

Therefore from Eqs. (B.59) and (B.60), compliance matrices of Links 2 and 3 can be expressed as,

$$\mathbf{C_{L_2 o, F_o}} = \mathbf{T_{-2\pi/3}} \times \mathbf{C_{L_1 o, F_o}} \times \mathbf{T^{T}_{-2\pi/3}} \tag{B.63}$$

$$\mathbf{C_{L_3 o, F_o}} = \mathbf{T_{2\pi/3}} \times \mathbf{C_{L_1 o, F_o}} \times \mathbf{T^{T}_{2\pi/3}} \tag{B.64}$$

B.5. Compliance matrix $\mathbf{C_{o,F_o}}$

Since Links 1, 2 and 3 are arranged parallel to each other (see Fig. 7), the compliance matrix of the 3-RRR compliant micro-motion stage, $\mathbf{C_{o,F_o}}$ can be found using the rule of calculating the equivalent compliances for parallel connections of springs.

$$\mathbf{C_{o,F_o}} = \left(\mathbf{C^{-1}_{L_1 o, F_o}} + \mathbf{C^{-1}_{L_2 o, F_o}} + \mathbf{C^{-1}_{L_3 o, F_o}}\right)^{-1} \tag{B.65}$$

The output displacements of the 3-RRR compliant stage due to applied forces/moments can be expressed as,

$$\begin{bmatrix} \Delta x_o \\ \Delta y_o \\ \Delta \alpha_o \end{bmatrix}_{3\mathrm{RRR}} = \mathbf{C_{o,F_o}} \times \mathbf{F_o} \tag{B.66}$$

B.6. Derivation of compliance matrix, $\mathbf{C_{o,F_{in}}}$ *and* $\mathbf{C_{in,F_o}}$

The compliance matrix which relates the output displacements at Point o to input forces $F_{1\mathrm{in}}$, $F_{2\mathrm{in}}$ and $F_{3\mathrm{in}}$ is,

$$\mathbf{C_{o,F_{in}}} = \begin{bmatrix} \mathbf{C_{o,F_{1in}}} & \mathbf{C_{o,F_{2in}}} & \mathbf{C_{o,F_{3in}}} \end{bmatrix} \tag{B.67}$$

where $\mathbf{C_{o,F_{1in}}}$, $\mathbf{C_{o,F_{2in}}}$ and $\mathbf{C_{o,F_{3in}}}$ are 3×1 matrices relating the output displacements to the input forces.

In order to find $\mathbf{C}_{\mathbf{o},\mathbf{F}_{1in}}$ in Eq. (B.67), the 3-RRR compliant stage is divided into three RRR links, similar to the calculation of $\mathbf{C}_{\mathbf{o},\mathbf{F}_{o}}$. The compliance matrix ($\mathbf{C}_{\mathbf{L}_1\mathbf{o}',\mathbf{F}_{1in}}$) of Link 1 at Point $o\prime$ due to F_{1in} is firstly calculated. Then, the compliance matrix at Point o, $\mathbf{C}_{\mathbf{L}_1\mathbf{o},\mathbf{F}_{1in}}$ are calculated by multiplying the transformation matrix, $\mathbf{T}_{\mathbf{d}}$ to $\mathbf{C}_{\mathbf{L}_1\mathbf{o}',\mathbf{F}_{1in}}$.

B.6.1. Derivation of $\mathbf{C}_{\mathbf{L}_1\mathbf{o}',\mathbf{F}_{1in}}$ *and* $\mathbf{C}_{\mathbf{L}_1\mathbf{o},\mathbf{F}_{1in}}$

When input force F_{1in} is applied, compliances of the RRR Link 1 at Point $o\prime$ and Point o are only affected by the compliances of Hinge 1 due to its open-chain configuration. The compliance matrix at Point $o\prime$, $\mathbf{C}_{\mathbf{L}_1\mathbf{o}',\mathbf{F}_{1in}}$ due to Hinge 1 is expressed as,

$$\mathbf{C}_{\mathbf{L}_1\mathbf{o}',\mathbf{F}_{1in}} = \begin{bmatrix} \partial\Delta x^1_{o'}/\partial F_{1in} \\ \partial\Delta y^1_{o'}/\partial F_{1in} \\ \partial\Delta\alpha^1_{o'}/\partial F_{1in} \end{bmatrix} \tag{B.68}$$

where the partial derivative terms in Eq. (B.68) are derived as follows:

The $\Delta\alpha^1_1$-, Δy^1_1- and Δx^1_1-compliances of Hinge 1 caused by F_{1in} are obtained by taking the partial derivatives of $\Delta\alpha^1_1$, Δy^1_1 and Δx^1_1 from Eqs. (B.9), (B.13) and (B.21) with respect to the input force F_{1in} acting at Point 1_{in} (see Fig. 8),

$$\frac{\partial\Delta\alpha^1_1}{\partial F_{1in}} = -(l_5+R_1)\left[\frac{\Delta\alpha_z}{M_z}\right]_1 \tag{B.69}$$

$$\frac{\partial\Delta y^1_1}{\partial F_{1in}} = -\left[\frac{\Delta y}{F_y}\right]_1 - (l_5R_1)\left[\frac{\Delta\alpha_z}{M_z}\right]_1 \tag{B.70}$$

$$\frac{\partial\Delta x^1_1}{\partial F_{1in}} = 0 \tag{B.71}$$

The $\Delta\alpha^1_{o'}$-displacement is the same as $\Delta\alpha^1_1$-displacement. Therefore, the partial derivative of $\Delta\alpha^1_{o'}$ with respect to F_{1in} ($\partial\Delta\alpha^1_{o'}/\partial F_{1in}$) are the same as Eq. (B.69).

The $\Delta y^1_{o'}$- and $\Delta x^1_{o'}$-compliances of Hinge 1 caused by F_{1in} are obtained by taking the partial derivatives of $\Delta y^1_{o'}$ (Eq. (B.17)) and $\Delta x^1_{o'}$ (Eq. (B.25)) with respect to F_{1in} at Point 1_{in},

$$\frac{\partial\Delta y^1_{o'}}{\partial F_{1in}} = \frac{\partial\Delta y^1_1}{\partial F_{1in}} + \frac{\partial\Delta\alpha^1_{o'}}{\partial F_{1in}}l_1 = -\left[\frac{\Delta y}{F_y}\right]_1 - \left\{(l_5R_1 + l_1(l_5+R_1))\left[\frac{\Delta\alpha_z}{M_z}\right]_1\right\} \tag{B.72}$$

$$\frac{\partial\Delta x^1_{o'}}{\partial F_{1in}} = \frac{\partial\Delta x^1_1}{\partial F_{1in}} - \frac{\partial\Delta\alpha^1_{o'}}{\partial F_{1in}}l_4 = l_4(l_5+R_1)\left[\frac{\Delta\alpha_z}{M_z}\right]_1 \tag{B.73}$$

By substituting Eqs. (B.69), (B.72) and (B.73) into Eq. (B.68), $\mathbf{C}_{\mathbf{L}_1\mathbf{o}',\mathbf{F}_{1in}}$ can be found.

The compliance matrix at Point o, $\mathbf{C}_{\mathbf{L}_1\mathbf{o},\mathbf{F}_{1in}}$ is,

$$\mathbf{C}_{\mathbf{L}_1\mathbf{o},\mathbf{F}_{1in}} = \mathbf{T}_{\mathbf{d}} \times \mathbf{C}_{\mathbf{L}_1\mathbf{o}',\mathbf{F}_{1in}} \tag{B.74}$$

B.6.2. Derivation of $\mathbf{C}_{\mathbf{o},\mathbf{F}_{1in}}$, $\mathbf{C}_{\mathbf{o},\mathbf{F}_{2in}}$ *and* $\mathbf{C}_{\mathbf{o},\mathbf{F}_{3in}}$

The output displacement of Link 1, $\mathbf{D}_{\mathbf{L}_1\mathbf{o},\mathbf{F}_{1in}}$ at Point o due to input force F_{1in} is,

$$\mathbf{D}_{\mathbf{L}_1\mathbf{o},\mathbf{F}_{1in}} = \mathbf{C}_{\mathbf{L}_1\mathbf{o},\mathbf{F}_{1in}} \times F_{1in} \tag{B.75}$$

By using Eq. (B.58), the output displacement of Link 1, $\mathbf{D}_{\mathbf{L}_1\mathbf{o},\mathbf{F}_{o}}$ at Point o due to output force $\mathbf{F}_{\mathbf{o}}$ is,

$$\mathbf{D}_{\mathbf{L}_1\mathbf{o},\mathbf{F}_{o}} = \mathbf{C}_{\mathbf{L}_1\mathbf{o},\mathbf{F}_{o}} \times \mathbf{F}_{\mathbf{o}} \tag{B.76}$$

By equating Eqs. (B.75) and (B.76), the equivalent output force $\mathbf{F}_{\mathbf{L}_1\mathbf{o},\mathbf{eqv}}$ at Point o when $F_{1in} = 1$N (unit force) can be calculated as below, where $\mathbf{F}_{\mathbf{L}_1\mathbf{o},\mathbf{eqv}} = \mathbf{F}_{\mathbf{o}}$ in Eq. (B.76).

$$\mathbf{F}_{\mathbf{L}_1\mathbf{o},\mathbf{eqv}} = \left[\mathbf{C}_{\mathbf{L}_1\mathbf{o},\mathbf{F}_{o}}\right]^{-1} \times \mathbf{C}_{\mathbf{L}_1\mathbf{o},\mathbf{F}_{1in}} \tag{B.77}$$

By multiplying the equivalent output force $\mathbf{F}_{\mathbf{L}_1\mathbf{o},\mathbf{eqv}}$ to $\mathbf{C}_{\mathbf{o},\mathbf{F}_{o}}$, the output displacement of the 3-RRR compliant stage caused by F_{1in} from Link 1 can be found. Since a unit force of F_{1in} is used to calculate the equivalent output force, the output displacement obtained can also represents the output compliance of the stage caused by F_{1in}

$$\mathbf{C}_{\mathbf{o},\mathbf{F}_{1in}} = \mathbf{D}_{\mathbf{o},\mathbf{F}_{1in}} = \mathbf{C}_{\mathbf{o},\mathbf{F}_{o}} \times \mathbf{F}_{\mathbf{L}_1\mathbf{o},\mathbf{eqv}} \tag{B.78}$$

Since Link 2 and Link 3 are orientated by $-120°$ and $120°$ from Link 1, $\mathbf{C}_{\mathbf{o},\mathbf{F}_{2in}}$ and $\mathbf{C}_{\mathbf{o},\mathbf{F}_{3in}}$ can be found as shown below.

$$\mathbf{C}_{\mathbf{o},\mathbf{F}_{2in}} = \mathbf{T}_{-2\pi/3} \times \mathbf{C}_{\mathbf{o},\mathbf{F}_{1in}} \tag{B.79}$$

$$\mathbf{C}_{\mathbf{o},\mathbf{F}_{3in}} = \mathbf{T}_{2\pi/3} \times \mathbf{C}_{\mathbf{o},\mathbf{F}_{1in}} \tag{B.80}$$

By substituting Eqs. (B.78)–(B.80) into Eq. (B.67), the compliance matrix $\mathbf{C}_{\mathbf{o},\mathbf{F}_{in}}$ of the 3-RRR stage can be obtained.

And $\mathbf{C}_{\mathbf{in},\mathbf{F}_{o}}$ is the transpose of $\mathbf{C}_{\mathbf{o},\mathbf{F}_{in}}$ and can be obtained as below,

$$\mathbf{C}_{\mathbf{in},\mathbf{F}_{o}} = \left[\mathbf{C}_{\mathbf{o},\mathbf{F}_{in}}\right]^{\mathrm{T}} \tag{B.81}$$

B.7. Derivation of compliance matrix, $\mathbf{C_{in,F_{in}}}$

The compliance matrix which relates the input displacements at Point 1_{in}, Point 2_{in} and Point 3_{in} to input forces F_{1in}, F_{2in} and F_{3in} is,

$$\mathbf{C_{in,F_{in}}} = \begin{bmatrix} \mathbf{C_{in,F_{1in}}} & \mathbf{C_{in,F_{2in}}} & \mathbf{C_{in,F_{3in}}} \end{bmatrix} \tag{B.82}$$

where $\mathbf{C_{in,F_{in}}}$ is a 3×3 matrix, $\mathbf{C_{in,F_{1in}}}$, $\mathbf{C_{in,F_{2in}}}$ and $\mathbf{C_{in,F_{3in}}}$ are 3×1 matrices.

The input displacements, $\mathbf{D_{in,F_{1in}}}$ due to input force F_{1in} can be calculated as below, where $\mathbf{C_{in,F_o}}$ is obtained from Eq. (B.81) and $\mathbf{F_{L_1o,eqv}}$ is obtained from Eq. (B.77). Note that $\mathbf{F_{L_1o,eqv}}$ is the equivalent force calculated at Point *o* when input force F_{1in} is applied at Link 1. Since a unit force of F_{1in} is used to obtain the equivalent output force, the input displacements $\mathbf{D_{in,F_{1in}}}$ obtained can also represents the input compliances of the stage caused by F_{1in}

$$\mathbf{C_{in,F_{1in}}} = \mathbf{D_{in,F_{1in}}} = \begin{bmatrix} u_{1in,F_{1in}} \\ u_{2in,F_{1in}} \\ u_{3in,F_{1in}} \end{bmatrix} = \mathbf{C_{in,F_o}} \times \mathbf{F_{L_1o,eqv}} \tag{B.83}$$

where $u_{1in,F_{1in}}$, $u_{2in,F_{1in}}$ and $u_{3in,F_{1in}}$ are displacements at Point 1_{in}, Point 2_{in} and Point 3_{in}(see Fig. 6) of the 3-RRR stage due to F_{1in}.

Similarly for Links 2 and 3,

$$\mathbf{C_{in,F_{2in}}} = \mathbf{D_{in,F_{2in}}} = \mathbf{C_{in,F_o}} \times \mathbf{F_{L_2o,eqv}} \tag{B.84}$$

where

$$\mathbf{F_{L_2o,eqv}} = \mathbf{T_{-2\pi/3}} \times \mathbf{F_{L_1o,eqv}}$$

and

$$\mathbf{C_{in,F_{3in}}} = \mathbf{D_{in,F_{3in}}} = \mathbf{C_{in,F_o}} \times \mathbf{F_{3o,eqv}} \tag{B.85}$$

where

$$\mathbf{F_{L_3o,eqv}} = \mathbf{T_{2\pi/3}} \times \mathbf{F_{L_1o,eqv}}$$

By substituting Eqs. (B.83)–(B.85) into Eq. (B.82), compliance matrix $\mathbf{C_{in,F_{in}}}$ can be obtained.

References

[1] F. Scire, E. Teague, Piezodriven 50-μm range stage with subnanometer resolution, Review of Scientific Instruments 49 (12) (1978) 1735–1740.
[2] E. Furukawa, M. Mizuno, T. Doi, Development of a flexure-hinged translation mechanism driven by two piezoelectric stacks, JSME International Journal Series, C: Dynamics Control, Robotics, Design, and Manufacturing 34 (4) (1995) 743–748.
[3] R. Yang, M. Jouaneh, R. Schweizer, Design and characterisation of a low-profile micropositioning stage, Precision Engineering 18 (1996) 20–29.
[4] M. Jouaneh, R. Yang, Modeling of flexure-hinge type lever mechanisms, Precision Engineering 27 (2003) 407–418.
[5] N. Lobontiu, E. Garcia, Analytical model of displacement amplification and stiffness optimization for a class of flexure-based compliant mechanisms, Computers and Structures 81 (2003) 2797–2810.
[6] S. Park, S. Yang, A mathematical approach for analysing ultra precision positioning system with compliant mechanism, Journal of Materials Processing Technology 164–165 (2005) 1584–1589.
[7] [7] S. Choi, S. Han, Y. Han, B. Thompson, A magnification device for precision mechanisms featuring piezoactuators and flexure hinges: design and experimental validation, Mechanism and Machine Theory 42 (9) (2007) 1184–1198.
[8] J.W. Ryu, D. Gweon, K.S. Moon, Optimal design of a flexure hinge based $xy\theta$ wafer stage, Precision Engineering 21 (1997) 18–28.
[9] H.-H. Pham, I.-M. Chen, Stiffness modeling of flexure parallel mechanism, Precision Engineering 29 (2005) 467–478.
[10] I. Her, J.C. Chang, A linear scheme for the displacement analysis of micropositioning stages with flexure hinges, Journal of Mechanical Design, Transactions ASME 116 (1994) 770–776.
[11] S. Smith, D. Chetwynd, D. Bowen, Design and assessment of monolithic high precision translation mechanisms, Journal of Physics E: Scientific Instruments 20 (1987) 977–983.
[12] N. Lobontiu, J.S. Paine, E. Garcia, M. Goldfarb, Design of symmetric conic-section flexure hinges based on closed-form compliance equations, Mechanism and Machine Theory 37 (2002) 477–498.
[13] S. Zhang, E.D. Fasse, A finite-element-based method to determine the spatial stiffness properties of a notch hinge, Journal of Mechanical Design 123 (2001) 141–147.
[14] W.O. Schotborgh, F.G. Kokkeler, H. Tragter, F.J. van Houten, Dimensionless design graphs for flexure elements and a comparison between three flexure elements, Precision Engineering 29 (2005) 41–47.
[15] J.M. Paros, L. Weisbord, How to design flexure hinges, Machine Design 37 (1965) 151–156.
[16] Y.K. Yong, T.-F. Lu, D.C. Handley, Review of circular flexure hinge design equations and derivation of empirical formulations, Precision Engineering 32 (2) (2008) 63–70.
[17] Y.K. Yong, T.-F. Lu, The effect of the accuracies of flexure hinge equations on the output compliances of planar micro-motion stages, Mechanism and Machine Theory 43 (2008) 347–363.
[18] N. Lobontiu, Compliant Mechanisms: Design of Flexure Hinges, CRC Press, 2003.
[19] D. Handley, T.-F. Lu, Y.K. Yong, A simple and efficient modelling method for planar flexure hinge compliant mechanisms, Precision Engineering, submitted for publication.
[20] W.-K. Kim, B.-J. Yi, W. Cho, RCC characteristics of planar/spherical three degree-of-freedom parallel mechanisms with joint compliances, Journal of Mechanical Design 122 (2000) 10–16.

[21] ANSYS, ANSYS Element Reference, ANSYS Inc., 2002.
[22] D.C. Handley, The modelling and optimal design of a three degree-of-freedom XYθ_z micro-motion stage, Ph.D. Thesis, The University of Adelaide, 2006.
[23] Y. Wu, Z. Zhou, Design calculations for flexure hinges, Review of Scientific Instruments 73 (8) (2002) 3101–3106.
[24] Y.M. Tseytlin, Notch flexure hinges: an effective theory, Review of Scientific Instruments 73 (9) (2002) 3363–3368.